MRL/MpJ-*Fas*^{lpr} mice show abnormalities in ovarian function and morphology with the progression of autoimmune disease

Yuki Otani[1], Osamu Ichii[1], Saori Otsuka-Kanazawa[1], Masataka Chihara[1], Teppei Nakamura[1, 2], Yasuhiro Kon[1]*

[1]Laboratory of Anatomy, Department of Biomedical Sciences, Graduate School of Veterinary Medicine, Hokkaido University; Sapporo, Japan

[2]Section of Biological Safety Research, Chitose Laboratory, Japan Food Research Laboratories; Chitose, Japan

*__Corresponding author:__ Yasuhiro Kon; Hokkaido University, Kita 18-Nishi 9, Kita ku; 060-0818 Sapporo, Japan; Tel: 011-706-5189; Email: y-kon@vetmed.hokudai.ac.jp

Running head: Ovary abnormalities in MRL/MpJ autoimmune mice

Keywords: MRL/lpr mice, autoimmune disease, ovary, estrous cycle, ovarian reserve

Abstract

The immune system is known to affect reproductive function, and maternal-fetal immune tolerance is essential for a successful pregnancy. To investigate the relationship between autoimmune disease and female reproductive function, we performed a comparative analysis of the ovarian phenotypes for C57BL/6 mice, autoimmune disease-prone MRL/MpJ (MRL/+) mice, and congenic MRL/MpJ-*Fas*^{lpr} (MRL/lpr) mice harboring a mutation in the *Fas* gene that speeds disease onset. Both MRL-background strains showed earlier vaginal opening than C57BL/6 mice. The estrous cycle became irregular by 6 and 12 months of age in MRL/lpr mice and mice of the other two strains, respectively. Histological analysis at 3 months revealed that the number of primordial follicles was smaller in MRL-background mice than in C57BL/6 mice after 3 months. In addition, MRL/lpr and MRL/+ mice displayed lower numbers of ovarian follicles and corpora lutea at 3 and 6 months, and 6 and 12 months, respectively, than that in age-matched C57BL/6 mice. MRL/lpr and MRL/+ mice developed ovarian interstitial glands after 3 and 6 months, respectively. In particular, MRL/lpr mice showed numerous infiltrating lymphocytes within the ovarian interstitia, and partially stratified ovarian surface epithelia with more developed microvilli than that observed in

C57BL/6 mice at 6 months. No significant differences in serum hormone levels were observed between the strains. In conclusion, MRL/lpr mice display altered ovarian development, morphology, and function consistent with the progression of severe autoimmune disease, as these findings are less severe in MRL/+ counterparts.

Introduction

In mammals, the female reproductive period is limited by the finite number of oocytes in the ovaries. In humans, the total number of oocytes gradually decreases with age due to physiological processes such as ovulation and follicular atresia. However, gonadal dysfunction, such as premature ovarian failure (POF), can cause an unexpected decrease in the number of oocytes stored in the ovaries. Patients with POF show amenorrhea, hypoestrogenism, and elevated serum levels of follicle-stimulating hormone (FSH) by 40 years of age [1]. An estimated 1.5 million patients are diagnosed with POF each year, and approximately 1% of women worldwide live with this disease [2, 3]. Several reports have suggested that POF is caused by genetic factors, infectious agents, or iatrogenic causes [1, 2]. However, approximately one-third of POF cases are attributable to autoimmune diseases [2]. Autoimmune-associated POF is characterized by lymphocytic oophoritis and/or by the presence of ovarian autoantibodies and is usually observed in conjunction with autoimmune diseases such as Addison's disease [1, 2, 4]. In most cases, it is difficult for patients with POF to reacquire fertility with ovulation of healthy oocytes [1, 2].

In healthy individuals, many immune cells are present in the ovaries, suggesting

57 that they play important roles in ovarian function in several species, such as rodents,
58 cows, sheep, pigs, and horses [5]. For example, many leukocytes, such as lymphocytes,
59 granulocytes, and macrophages, are found in the corpora lutea in rodents, cows, and
60 horses. Furthermore, the number and type of immune cells present in corpora lutea
61 change with the estrous cycle, suggesting that these leukocytes participate in the
62 development and regression of corpora lutea [6, 7, 8]. In addition to immune cells, a
63 variety of cytokines and their receptors are expressed in the ovaries, indicating that they
64 play important roles in the control of ovarian function [9]. For example, interleukin 6
65 (IL-6) is expressed in granulosa cells, where it regulates the expression of the
66 luteinizing hormone (LH) receptor in rats [10]. Additionally, interleukin-1 (IL-1)
67 signaling via IL-1β and its receptor are essential for ovarian folliculogenesis and
68 ovulation in equine ovaries [11]. In pigs, tumor necrosis factor alpha (TNFα) acts as a
69 survival factor for granulosa cells during follicular atresia [12]. Furthermore, several
70 studies in clinical veterinary medicine also support the notion that altered immune
71 function may affect reproductive function. Briefly, dogs suffering autoimmune-mediated
72 thyroiditis are anestrous, suggesting a loss of reproductive function [13]. In laboratory
73 animals, autoimmune regulator (*Aire*)-deficient mice, which show severe autoimmune
74 phenotypes, are infertile, with follicular depletion and lymphocyte infiltration in their

ovaries [3]. Furthermore, the pathogenesis of autoimmune disease is influenced by the production of sex steroid hormones in the gonads; in particular, estrogen aggravates systemic lupus erythematosus (SLE) in humans and rodent models [14, 15]. These data suggest a close relationship between immune and reproductive function in mammals.

BXSB/MpJ-*Yaa*, NZBWF1, and MRL/MpJ-*Fas*^{lpr} (MRL/lpr) mice are used as autoimmune disease models, and their pathology resembles that of human SLE and rheumatoid arthritis [16, 17]. MRL/lpr mice show a much more severe autoimmune phenotype than congenic MRL/MpJ (MRL/+) mice, which results from the lymphoproliferation (*lpr*) mutation of *Fas* that causes abnormal survival of auto-reactive T lymphocytes [18]. In addition to the *lpr* mutation, the MRL background is prone to the development of autoimmune diseases, as it carries at least 13 disease susceptibility loci associated with the development of SLE-related diseases [19, 20, 21]. The onset of SLE is usually characterized by splenomegaly, autoantibody production, and glomerulonephritis. Accordingly, spleen weights significantly correlated with the serum autoantibody levels in MRL background strain [22], supporting their use as indicators of disease severity. Interestingly, MRL mice also manifest several unique phenotypes in the female reproductive organs [23, 24]. In particular, neonatal MRL/+ mice show accelerated folliculogenesis associated with the appearance of numerous mast cells in

93 the ovary [24]. Further, adult MRL/+ mice frequently develop ovarian cysts, originating
94 from the rete ovarii [23]. Although MRL/+ mice show several abnormalities in both
95 immune and reproductive function, the pathological and etiological correlations remain
96 unclear.

97 In this study, we used MRL-background mice to evaluate the relationship between
98 autoimmune disease and female reproductive function. Female MRL/lpr mice showed
99 abnormalities not only of ovarian function but also of morphology, characterized by
100 early loss of the estrous cycle accompanied by a significant increase in spleen weight.
101 These findings indicate that severe autoimmune disease affects female reproductive
102 function, and provide novel insights into the treatment of infertility derived from
103 immune system disruption.

Methods

Animal and sample preparation

Female C57BL/6, MRL/+, and MRL/lpr mice were purchased from Japan SLC, Inc. (Hamamatsu, Japan). Mice were maintained according to *The Guide for the Care and Use of Laboratory Animals of Hokkaido University, Graduate School of Veterinary Medicine* (approved by the Association for Assessment and Accreditation of Laboratory Animal Care International). Virgin female mice at 3, 6, 9, and 12 months of age were used at the metestrus stage of the estrous cycle, as determined by monitoring vaginal smears. Body weights were measured, and then blood samples were collected by cutting vena cava under deep anesthesia (Avertin; 2,2,2-tribromoethanol dissolved in 2-methyl-2-butanol, 2.4 g/kg, administered intraperitoneally). After mice were euthanized by cervical dislocation, the ovaries and spleen were collected. Spleen weight was measured, and the spleen weight to body weight ratio was calculated as an index of autoimmune disease progression.

Examination of vaginal opening and estrous cycles

The vaginal opening status was monitored in all mice as an indicator of the onset of puberty. After vaginal opening, vaginal smears were collected for 10 consecutive days every month until 12 months of age to assess estrous cyclicity. Properties of epithelial cells, leukocytes, and vaginal mucus were used to characterize each stage, as follows: “proestrus” was characterized by the appearance of round and nucleated epithelial cells without leukocytes; “estrus” was characterized by clustered and keratinized squamous epithelial cells; “metestrus” was characterized by a large number of leukocytes; and “diestrus” was characterized by low numbers of leukocytes and the presence of vaginal mucus. Metestrus was included in diestrus based on a previous report [25].

Histological analyses

Collected ovaries were fixed in 4% paraformaldehyde/0.1 M phosphate buffer (PB) overnight, embedded in paraffin, and cut into sections (3 μm thick). Deparaffinized sections were stained with hematoxylin-eosin (HE) or periodic acid-Schiff (PAS) for evaluation of ovarian morphology. The number of primordial, primary, secondary, and antral follicles was counted in five sections, and only follicles containing oocytes with an apparent nucleus were counted. The number of corpora lutea was also counted in five

sections. Finally, the total number counted in all five sections was used as the value for the respective ovary.

Some sections were immunostained using the following procedure: for antigen retrieval, sections were incubated in 20 mM Tris-HCl (pH 9.0) for 20 min at 105°C (CD3) or 0.05% trypsin/0.01 M phosphate-buffered saline (PBS, pH 7.4) for 5 min at 37°C (B220). The samples were then soaked in methanol containing 0.3% H_2O_2 to block internal peroxidase activity. Sections blocked in 10% normal goat serum for 30 min at room temperature were incubated with rat anti-B220 (1:1,600, Cedarlane, Ontario, Canada) or rabbit anti-CD3 (1:200, Nichirei, Tokyo, Japan) at 4°C overnight. After washing three times in PBS, sections were incubated with biotin-conjugated goat anti-rat IgG antibody (Caltag-Medsystems Limited, Buckingham, UK) for B220, or biotin-conjugated goat anti-rabbit IgG antibody (SABPO Kit, Nichirei, Tokyo, Japan), for 30 min at room temperature, washed again, and incubated with streptavidin-biotin complex (SABPO Kit, Nichirei) for 30 min. The sections were then incubated with 3,3'-diaminobenzidine tetrahydrochloride-H_2O_2 solution. Finally, the sections were lightly counterstained with hematoxylin. The number of CD3-positive cells in each immunostained section was counted, and the total number in five sections was used as the value for the respective ovary.

157

158 **Ultrastructural analysis**

159 For scanning electron microscopy (SEM), halves of glutaraldehyde-fixed ovaries
160 were placed in 2% tannic acid for 1 h at 4°C and postfixed with 1% osmium tetroxide in
161 0.1 M PB for 1 h. Specimens were dehydrated through a series of graded alcohols,
162 transferred into 3-methylbutyl acetate, and dried using an HCP-2 critical point dryer
163 (Hitachi, Tokyo, Japan). The dried specimens were sputter-coated using a Hitachi
164 E-1030 ion sputter coater (Hitachi) and then examined on an S-4100 SEM (Hitachi)
165 with an accelerating voltage of 5 kV.

166 For transmission electron microscopy (TEM), the ovaries of C57BL/6 and
167 MRL/lpr mice at 6 months were fixed with 2.5% glutaraldehyde in 0.1 M PB for 4 h.
168 Tissues were post-fixed with 1% osmium tetroxide in 0.1 M PB for 2 h, dehydrated
169 using a series of graded alcohols, and embedded in epoxy resin (Quetol 812 Mixture;
170 Nisshin EM, Tokyo, Japan). Semi-thin sections (0.5 μm thick) were stained with 1%
171 toluidine blue and examined. Ultra-thin sections (70 nm thick) were double-stained with
172 uranyl acetate and lead citrate and observed under a JEOL TEM (JEM-1210; JEOL,
173 Tokyo, Japan).

174

Measurement of serum hormone levels

Collected blood was centrifuged at 885 × *g* for 15 min. After clotted blood was removed, the samples were centrifuged at 22,136 × *g* for 5 min, and the supernatant was immediately frozen at -80°C. Serum levels of endogenous mouse FSH and testosterone were measured using ELISA kits (Endocrine Technologies Inc., Newark, USA) according to the manufacturer's instructions. All samples were tested in duplicate.

Statistical analysis

The results are expressed as the mean ± standard error (SE) and were analyzed using non-parametric statistical methods. The Kruskal-Wallis test was used to compare numerical results, and multiple comparisons were performed using Scheffe's method when significant differences were observed ($P < 0.05$).

Results

Autoimmune disease symptoms of mice

The spleen weight to body weight ratio was used as an index of autoimmune disease in mice (Figure 1). At all ages examined, MRL/lpr mice showed significantly higher values than the other two strains ($P < 0.05$). At 9 and 12 months, although MRL/+ mice showed slightly higher values than C57BL/6 mice, no significant differences were observed between C57BL/6 and MRL/+ mice.

Onset of puberty and estrous cyclicity of mice

Vaginal opening was observed in C57BL/6, MRL/+, and MRL/lpr mice to determine the onset of puberty (Figure 2). Vaginal opening occurred significantly earlier in MRL/+ (18.8 ± 4.3 days) and MRL/lpr mice (19.8 ± 1.7 days) than in C57BL/6 mice (39.6 ± 2.9 days) (Figure 2) ($P < 0.05$).

Age-related changes in estrous cyclicity were examined next (Figure 3). Figure 3A shows the representative pattern of mouse estrous cycle in each of the three strains at 3, 6, 9, and 12 months. C57BL/6 and MRL/+ mice showed regular cyclicity, with each cycle lasting 4–7 days until 9 months of age. These strains showed regular cyclicity

until 11 months of age (data not shown). However, MRL/lpr mice lost cyclicity after 6 months, characterized by a prolonged diestrus period and a shortened estrus period.

Figure 3B and C show the proportion of time spent in estrus and diestrus for each of the three strains. Estrus was significantly shorter in MRL/lpr mice than in the other strains at 6 months of age ($P < 0.05$). At 12 months, C57BL/6 and MRL/+ mice tended to show shorter and longer periods of estrus, respectively, compared to earlier months; however, no significant differences were observed among strains (Figure 3B). In addition, diestrus was longer in MRL/lpr mice at 6 months of age than in the other strains ($P < 0.05$). At 12 months, C57BL/6 and MRL/lpr mice showed longer periods of diestrus than in earlier months, but no significant differences were observed among strains (Figure 3C).

Age-related histological changes in mouse ovaries

Figure 4 shows the ovarian histology of C57BL/6, MRL/+, and MRL/lpr mice at 3, 6, and 12 months. At 3 months, follicles at various stages of development were observed at the ovarian cortices in all three strains (Figure 4A, D, and G); the number tended to decrease with age (Figure 4B, C, E, F, H, and I). In particular, very few follicles were observed in MRL/lpr mice at 12 months (Figure 4I). At all ages examined, a large

number of corpora lutea were observed in C57BL/6 and MRL/+ mice (Figure 4A–F); however, few were observed in MRL/lpr mice (Figure 4G–I). Further, the ovarian interstitium was larger in MRL/lpr mice (Figure 4G–I) than in the other strains.

Next, we quantified the number of follicles at each stage of follicular development (primordial, primary, secondary, and antral) and the number of corpora lutea at 3, 6, and 12 months of age in all three strains. The total number of follicles decreased with age in all strains (Figure 4J–L), and the number of follicles observed at each stage differed among strains and at different ages of the mice. Briefly, MRL/+ and MRL/lpr mice showed a smaller number of primordial follicles than C57BL/6 mice at all ages examined, and significant differences between strains were observed at 3 and 6 months (Figure 4J–K) ($P < 0.05$). Further, MRL/+ mouse ovaries contained a significantly larger number of secondary follicles than the other two strains at 3 months (Figure 4J) ($P < 0.05$). The total number of follicles was significantly lower in MRL/lpr mice than in the other two strains at 3 months, and in both MRL/+ and MRL/lpr mice than in C57BL6 mice at 6 months (Figure 4J–K) ($P < 0.05$). In addition, the number of corpora lutea was lowest in MRL/lpr mice at all ages examined; it was also significantly lower in MRL/+ than in C57BL/6 mice at 12 months (Figure 4M) ($P < 0.05$).

As shown in Figure 5, strain-related differences in ovarian morphology were

241 observed at the ovarian interstitium and on the ovarian surface. The ovarian interstitium
242 contains interstitial glands comprised of interstitial endocrine cells (IECs) (Figure 5A–I).
243 These IECs originate from internal theca or granulosa cells of atretic follicles and
244 primarily produce testosterone in rodents [26]. IECs were clearly observed in C57BL/6
245 mice at 12 months (Figure 5C) and in MRL/+ mice after 6 months (Figure 5E–F).
246 However, large numbers of IECs were clearly present in MRL/lpr mouse ovaries at all
247 ages examined (Figure 5G–I). Finally, the ovarian surface epithelium (OSE) was a
248 squamous monolayer in C57BL/6 and MRL/+ mice at all ages examined (Figure 5J–K),
249 whereas a partially cuboidal, stratified epithelium was observed in MRL/lpr mice after 6
250 months (Figure 5L).
251
252 **Ultrastructure of the ovarian surface**
253 The morphology of the ovarian surface was compared between C57BL/6 and
254 MRL/lpr mice at 6 months by using electron microscopy. Under SEM observation, the
255 ovarian surface of C57BL/6 mice appeared smooth (Figure 6A) and was mostly covered
256 with oval- or spindle-shaped epithelial cells with microvilli (Figure 6B). In contrast, the
257 ovarian surface of MRL/lpr mice showed several dome-shaped bulges (Figure 6C)
258 covered by rounded epithelial cells that were fully covered in microvilli (Figure 6D).

259 The microvillus density of epithelial cells appeared to be higher in MRL/lpr mice than
260 in C57BL/6 mice (Figure 6B and D).

261 Next, the ovarian surface was observed using semi-thin and ultra-thin sections
262 (Figure 6E–H). In C57BL/6 mice, the OSE consisted of monolayered dark- or
263 pale-colored cells (Figure 6E). Under TEM, the dark-colored cells in semi-thin sections
264 showed a highly electron-dense cytoplasm and few microvilli, whereas the pale-colored
265 cells had a cytoplasm with low electron density and a large round nucleus similar to that
266 found in oocytes (Figure 6F). Likewise, two cell types were observed in the semi-thin
267 OSE sections of MRL/lpr mice (Figure 6G). However, the OSE cells and ovarian tunica
268 albuginea (lowermost layer of the ovary capsule) were taller and thicker, respectively, in
269 MRL/lpr mice than in C57BL/6 mice (Figure 6E and G), which was also accompanied
270 by an increase in the presence of collagen fibrils (Figure 6H). Under TEM, the
271 dark-colored cells in the semi-thin sections showed a highly electron-dense cytoplasm
272 and abundant microvilli in MRL/lpr mice (Figure 6H). The pale-colored cells in
273 semi-thin sections had a cytoplasm with low electron density and a larger nucleus than
274 the dark-colored cells (Figure 6H). The microvillus density of cells with a highly
275 electron-dense cytoplasm in MRL/lpr mice appeared to be higher than that in C57BL/6
276 mice (Figure 6F and H), as well as in cells of MRL/lpr mice with a cytoplasm with low

electron density (Figure 6H).

Inflammatory cell infiltration in mouse ovaries

Immunohistochemical analysis was used to detect T and B cells in the ovaries of C57BL/6, MRL/+, and MRL/lpr mice (Figure 7). At 6 months, few CD3-positive T cells were observed in the ovaries of C57BL/6 and MRL/+ mice, which tended to localize in or around the corpora lutea (Figure 7A and B). However, numerous CD3-positive T cells were observed in the ovaries of MRL/lpr mice (Figure 7C). These cells were widely distributed, and mainly localized to the ovarian interstitium (Figure 7C). Quantification of CD3-positive T cells in the ovaries showed that MRL/lpr mice showed significantly higher values than the other two strains at both 3 and 6 months of age (Figure 7D) ($P < 0.05$). At 3 months, CD3-positive T cells were observed in or around the follicles of MRL/lpr mice (Figure 7E–F). Further, few B220-positive B cells were observed in the ovaries of C57BL/6 and MRL/+ mice at any period examined (Figure 7G–H), whereas some MRL/lpr mice showed numerous positive cells in the ovarian interstitium at 6 months (Figure 7I).

Serum levels of FSH and testosterone in mice

We next compared the blood serum levels of FSH and testosterone—indicators of reproductive ability and IEC function, respectively—in C57BL/6, MRL/+, and MRL/lpr mice at 6 and 12 months (Figure 8) [26, 27]. Although serum FSH levels tended to be slightly higher in MRL/lpr mice than in C57BL/6 and MRL/+ mice at 12 months, no significant differences among strains were observed at any age (Figure 8A). Similar to FSH, serum testosterone levels were higher in MRL/lpr mice than in C57BL/6 and MRL/+ mice at 6 and 12 months, but the differences were not significant (Figure 8B).

Discussion and Conclusions

Several studies have indicated a close correlation between the immune and reproductive systems [5, 9]. This study examined the effect of autoimmune disease on ovarian morphology using MRL-background mouse strains. From 3 months, MRL/lpr mice showed autoimmune defects, indicated by significantly increased spleen weight compared to MRL/+ and C57BL/6 mice. At the same age, the total number of follicles and corpora lutea tended to be smaller in MRL/lpr mice than in mice of other strains. Further, numerous IEC and infiltrating lymphocytes were observed in MRL/lpr mouse ovaries. Importantly, lymphocytic oophoritis with loss of the follicle pool has also been reported in autoimmune-mediated POF [1, 2, 4]. Although the MRL background carries several susceptibility loci associated with the development of autoimmune defects [19, 20], changes in ovarian morphology and development of autoimmune disease were less pronounced in MRL/+ mice than in MRL/lpr mice. Further, some MRL/+ and MRL/lpr mice developed ovarian cysts, as reported previously [23]; however, no correlation between cyst development and the parameters evaluated was found in this study (data not shown). Importantly, our data indicates that splenomegaly (3 months) precedes the onset of estrous cycle irregularity (6 months) in MRL/lpr mice. Therefore, the *lpr*

mutation and/or its associated autoimmune defects may be crucial to the changes in ovarian morphology observed in MRL-background strains.

It has been proposed that granulosa cells or oocytes may form from the mesodermal OSE [28, 29]. In this study, both dark- and pale-colored cells were observed in semi-thin sections of the OSE. The pale cells were likely oocytes or their progenitors, considering their nuclear shape and previous reports [28]. The OSE showed a unique morphology in MRL/lpr mice but not in MRL/+ or C57BL/6 mice at 6 months. Ultrastructurally, the microvilli were more developed in MRL/lpr mice than in C57BL/6 mice, as shown by SEM examination of the OSE and TEM observation of dark-colored cells, and the OSE was partially stratified in MRL/lpr mice. Although no clear evidence elucidating the mechanism for altering OSE structures was found, altered morphology of the peritoneal mesothelium has been reported in ascitic conditions—such as intraperitoneal dialysis [30]. Further, patients with autoimmune diseases or ovarian cancer show altered amounts or components of ascitic fluid [31, 32]. Therefore, the features of OSE in MRL/lpr mice may reflect an altered environment in or around the ovaries.

Further, only MRL/lpr mice showed a thickened ovarian tunica albuginea similar to that reported in patients with polycystic ovarian syndrome and in model mice [33, 34].

Thickening of the tunica albuginea could contribute to infertility by disturbing ovulation. In this study, the ability of MRL/lpr mice to ovulate or become pregnant remains unclear; however, evaluation of the tunica albuginea may be important to elucidate the pathogenesis of ovulation disorders in autoimmune diseases, such as autoimmune-mediated POF.

MRL/lpr mice showed an irregular estrous cycle associated with the significant increase of spleen weights and morphological changes in the ovaries beginning at 6 months of age. The estrous cycle progresses through folliculogenesis, ovulation, and luteinization [35]. These processes are coordinated by oocytes, follicular epithelial cells/granulosa cells, and lutein cells via the interaction of gonadotropins such as LH and FSH [35]. Furthermore, loss of the follicle pool and elevated serum FSH levels are pathological characteristics in human patients with POF showing an altered menstrual cycle [14]. In this study, no significant differences were observed in serum levels of FSH among strains, but MRL/lpr mice showed significantly decreased numbers of follicles and corpora lutea. Therefore, abnormal populations of ovarian functional units—such as follicles and corpora lutea—rather than serum gonadotropin levels, may have greater impact on the cyclicity of the estrous cycle in this murine autoimmune disease model.

In this study, MRL/+ and MRL/lpr mice showed several common phenotypes, such as earlier vaginal opening and fewer primordial follicles than C57BL/6 mice, despite the significant increase of spleen weights observed in MRL/+ mice. A previous study suggested that MRL/+ mice showed enhanced progression through early folliculogenesis than C57BL/6 mice [22, 36]. Therefore, the earlier onset of puberty and fewer primordial follicles compared to C57BL/6 mice are unique phenotypes in MRL-background strains.

However, the appearance of MRL-derived unique ovarian phenotypes differed between MRL/+ and MRL/lpr mice in several ways. Briefly, MRL/+ mouse ovaries contained a larger number of secondary follicles than those of MRL/lpr mice at 3 months. Further, compared to C57BL/6 mice, the total number of follicles was smaller from 3 and 6 months in MRL/lpr and MRL/+ mice, respectively. These results suggest that the unique phenotypes associated with folliculogenesis in MRL/+ mice were altered in MRL/lpr mice. Moreover, MRL/lpr mice exhibited an increased infiltration of T cells in or around follicles after 3 months of age, suggesting that these cells or their derived cytokines may affect folliculogenesis.

Testosterone-producing IECs originate from internal theca cells or granulosa cells of atretic follicles and develop in the ovarian interstitium of rodents [26]. In this study,

374 although the number of corpora lutea was smaller, the number of IECs in the ovaries of
375 MRL/lpr mice was increased after 3 months, and a similar tendency was observed in
376 older MRL/+ mice. Therefore, the MRL background may contribute to the development
377 of IECs in both MRL/+ and MRL/lpr mice. Further, the serum testosterone
378 concentration tended to be higher in MRL/lpr mice than in mice of the other strains,
379 possibly reflecting the development of IECs in MRL/lpr mice.

380 In mammalian ovaries, the development and regression of corpora lutea is
381 regulated by cytokines produced by immune cells observed in or around corpora lutea
382 via NFκB signaling [5, 9]. In the present study, few lymphocytes were observed in or
383 around the corpora lutea of C57BL/6 and MRL/+ mice. In contrast, a pronounced
384 infiltration of B and T cells into the ovarian interstitium was observed in MRL/lpr mice.
385 Furthermore, previous reports have suggested that granulosa cells and theca cells
386 express Fas, and that Fas-Fas ligand-mediated apoptosis is important for the regression
387 of corpora lutea [37, 38]. Based on these findings, we suggest that changes in the local
388 immune microenvironment and/or cell death resulting from *lpr* mutation in the *Fas* gene
389 may affect the differentiation of internal theca cells/granulosa cells into IECs.

390 In conclusion, we demonstrated a relationship between ovarian morphology and
391 reproductive function in MRL/lpr autoimmune mice. These data may aid in clarifying

392 the pathogenic mechanism of ovarian dysfunction in autoimmune disease. Briefly,
393 intraovarian infiltration of immune cells, loss of the follicle pool, and a disrupted
394 estrous cycle are common pathological features of autoimmune disease between POF
395 patients and MRL/lpr mice. While MRL/lpr mice did not clearly exhibit the increased
396 levels of FSH characteristic of POF, they did display unique ovarian phenotypes
397 including failures in follicle luteinization, increased IECs, and altered ovarian surface
398 morphology. Menstrual abnormalities, increased cycle length, and decreased serum
399 levels of hormones produced by corpora lutea were observed in patients with SLE [39,
400 40]. Ovarian reserve markers such anti-Müllerian hormone and antral follicle count
401 were decreased in adult patients with childhood-onset SLE [41]. In MRL/lpr mice, early
402 onset puberty and altered follicular development were observed for the same time or
403 earlier than the development of autoimmune defects indicated by increased spleen
404 weight. Importantly, it was reported that early age at menarche is associated with an
405 increased risk of SLE in human patients [42]. Taken collectively, we conclude that the
406 *Fas* mutation and subsequent immune defects triggered in the MRL background likely
407 leads to the abnormal reproductive phenotypes observed in MRL/lpr mice. This
408 complexity causes the phenotypic similarities and differences observed between
409 MRL/lpr mice and human clinical cases. This study provides a novel insight into the

410 treatment of infertility resulting from disruption of the immune system.

411

Acknowledgments

This work was partially supported by a Grant-in-Aid for Scientific Research (B) (No. 24380156).

Declaration of Interest

The authors declare that they have no competing interests.

References

1. Silva, C. A., L. Y. Yamakami, N. E. Aikawa, D. B. Araujo, J. F. Carvalho, and E. Bonfá. 2014. Autoimmune primary ovarian insufficiency. *Autoimmun. Rev.* 13: 427–430.
2. Goswami, D. and G. S. Conway. 2007. Premature ovarian failure. *Horm. Res*. 68: 196–202.
3. Jasti, S., B. D. Warren, L. K. McGinnis, W. H. Kinsey, B. K. Petroff, and M. G. Petroff. 2012. The autoimmune regulator prevents premature reproductive senescence in female mice. *Biol. Reprod.* 86: 110.
4. Kalantaridou, S. N., D. T. Braddock, N. J. Patronas, and L. M. Nelson. 1999. Treatment of autoimmune premature ovarian failure. *Hum. Reprod*. 14: 1777–1782.

5. Walusimbi, S. S. and J. L. Pate. 2013. Physiology and Endocrinology Symposium: role of immune cells in the corpus luteum. *J. Anim. Sci*. 91: 1650–1659.

6. Komatsu, K., N. Manabe, M. Kiso, M. Shimabe, and H. Miyamoto. 2003. Changes in localization of immune cells and cytokines in corpora lutea during luteolysis in murine ovaries. *J. Exp. Zool. A Comp. Exp. Biol*. 296: 152–159.

7. Lawler, D. F., J. Hopkins, and E. D. Watson. 1999. Immune cell populations in the equine corpus luteum throughout the oestrous cycle and early pregnancy: an immunohistochemical and flow cytometric study. *J. Reprod. Fertil*. 117: 281–290.

8. Penny, L. A., D. Armstrong, T. A. Bramley, R. Webb, R. A. Collins, and E. D. Watson. 1999. Immune cells and cytokine production in the bovine corpus luteum throughout the oestrous cycle and after induced luteolysis. *J. Reprod. Fertil*. 115: 87–96.

9. Sirotkin, A. V. 2011. Cytokines: Signaling molecules controlling ovarian functions. *Int. J. Biochem. Cell Biol*. 43: 857–861.

10. Imai, F., H. Kishi, K. Nakao, T. Nishimura, and T. Minegishi. 2014. IL-6 up-regulates the expression of rat LH receptors during granulosa cell differentiation. *Endocrinology* 155: 1436–1444.

11. Martoriati, A. and N. Gérard. 2003. Interleukin-1 (IL-1) system gene expression in

granulosa cells: kinetics during terminal preovulatory follicle maturation in the mare. *Reprod. Biol. Endocrinol*. 1: 42.

12. Nakayama, M., N. Manabe, N. Inoue, T. Matsui, and H. Miyamoto. 2003. Changes in the expression of tumor necrosis factor (TNF) α, TNFα receptor (TNFR) 2, and TNFR-associated factor 2 in granulosa cells during atresia in pig ovaries. *Biol. Reprod*. 68: 530–535.
13. Tizard, I. R. 2011. Organ-specific autoimmune disease. In *Veterinary Immunology: An Introduction*, 7th ed. T. Tada, S. Furusawa, and M. Yasuda, eds. Interzoo, Tokyo. p. 366–378 (in Japanese).
14. Hughes, G. C. and D. Choubey. 2014. Modulation of autoimmune rheumatic diseases by oestrogen and progesterone. *Nat. Rev. Rheumatol.* 10: 740–751.
15. Lee, T. P. and B. L. Chiang. 2012. Sex differences in spontaneous versus induced animal models of autoimmunity. *Autoimmun. Rev.* 11: A422–A429.
16. Nose, M., M. Terada, M. Nishihara, J. Kamogawa, T. Miyazaki, W. Qu, S. Mori, and S. Nakatsuru. 2000. Genome analysis of collagen disease in MRL/lpr mice: polygenic inheritance resulting in the complex pathological manifestations. *Int. J. Cardiol.* 75: S53–S61.
17. Theofilopoulos, A. N. and F. J. Dixon. 1985. Murine models of systemic lupus

erythematosus. *Adv. Immunol*. 37: 269–390.

18. Takahashi, T., M. Tanaka, C. I. Brannan, N. A. Jenkins, N. G. Copeland, T. Suda, and S. Nagata. 1994. Generalized lymphoproliferative disease in mice, caused by a point mutation in the Fas ligand. *Cell* 76: 969–976.

19. Ichii, O., A. Konno, N. Sasaki, D. Endoh, Y. Hashimoto, and Y. Kon. 2008. Autoimmune glomerulonephritis induced in congenic mouse strain carrying telomeric region of chromosome 1 derived from MRL/MpJ. *Histol. Histopathol.* 23: 411–422.

20. Santiago-Raber, M. L., C. Laporte, L. Reininger, and S. Izui. 2004. Genetic basis of murine lupus. *Autoimmun. Rev.* 3: 33–39.

21. Gu, L., A. Weinreb, X. P. Wang, D. I. Zack, J. H. Qiao, R. Weisbart, and A. J. Lusis. 1998. Genetic determinants of autoimmune disease and coronary vasculitis in the MRL-lpr/lpr mouse model of systemic lupus erythematosus. *J. Immunol.* 161: 6999–7006.

22. Vidal, S, D. H. Kono, and A. N. Theofilopoulos. 1998. Loci predisposing to autoimmunity in MRL-Fas lpr and C57BL/6-Faslpr mice. *J. Clin. Invest.* 101: 696–702.

23. Lee, S. H., O. Ichii, S. Otsuka, Y. H. Elewa, Y. Namiki, Y. Hashimoto, and Y. Kon.

2011. Ovarian cysts in MRL/MpJ mice are derived from the extraovarian rete: a developmental study. *J. Anat.* 219: 743–755.

24. Nakamura, T., S. Otsuka, O. Ichii, Y. Sakata, K. Nagasaki, Y. Hashimoto, and Y. Kon. 2013. Relationship between numerous mast cells and early follicular development in neonatal MRL/MpJ mouse ovaries. *PLoS One* 8: e77246.

25. Tello, J. A., T. Kohout, R. Pineda, R. A. Maki, R. Scott Struthers, and R. P. Millar. 2013. Reproductive physiology of a humanized GnRH receptor mouse model: application in evaluation of human-specific analogs. *Am. J. Physiol. Endocrinol. Metab*. 305: E67–E77.

26. Manabe, N. and J. Kimura. 2008. Female genital organ. In *Textbook of Veterinary Histology,* 4th ed. Japanese Association of Veterinary Anatomists, eds, Gakusousha, Tokyo. p. 19–208 (in Japanese).

27. Kinoshita, Y. and T. Yamamoto. 2000. Menopause and ovarian aging. *Nippon Sanka Fujinka Gakkai Zasshi*, 52: N-345–348 (in Japanese).

28. Celik, O., E. Celik, I. Turkcuoglu, E. Yilmaz, Y. Simsek, and B. Tiras. 2012. Germline cells in ovarian surface epithelium of mammalians: a promising notion. *Reprod. Biol. Endocrinol*. 10: 112.

29. Mork, L., D. M. Maatouk, J. A. McMahon, J. J. Guo, P. Zhang, A. P. McMahon, and

B. Capel. 2012. Temporal differences in granulosa cell specification in the ovary reflect distinct follicle fates in mice. *Biol. Reprod.* 86: 37.

30. Jovanović, N., S. Zunić-Bozinovski, D. Trpinac, S. Krstić, D. Oprić, J. Trbojević-Stanković, and B. Stojimirović. 2013. Ultrastructural changes of the peritoneum in a rabbit model of peritoneal dialysis. *Vojnosanit. Pregl.* 70: 1023–1028.

31. Ahmed, N. and K. L. Stenvers. 2013. Getting to know ovarian cancer ascites: opportunities for targeted therapy-based translational research. *Front. Oncol.* 3: 256.

32. Lee, C. K., J. M. Han, K. N. Lee, E. Y. Lee, J. H. Shin, Y. S. Cho, Y. Koh, B. Yoo, and H. B. Moon. 2002. Concurrent occurrence of chylothorax, chylous ascites, and protein-losing enteropathy in systemic lupus erythematosus. *J. Rheumatol.* 29: 1330–1333.

33. Devin, J. K., J. E. Johnson, M. Eren, L. A. Gleaves, W. S. Bradham, J. R. Jr. Bloodworth, and D. E. Vaughan. 2007. Transgenic overexpression of plasminogen activator inhibitor-1 promotes the development of polycystic ovarian changes in female mice. *J. Mol. Endocrinol.* 39: 9–16.

34. Irahara, M. 2008. New diagnosis criteria of PCOS in Japan. *Nippon Sanka Fujinka*

Gakkai Zasshi, 60: N-185–190 (in Japanese).

35. Katagiri, S. 2012. Female reproductive physiology. In *Textbook of Theriogenology*, 4th ed. T. Nakao, S. Tsumagari and S. Katagiri, eds. Buneido, Tokyo, p. 71–73 (in Japanese).

36. Yamashita, Y., T. Nakamura, S. Otsuka-Kanazawa, O. Ichii, and Y. Kon. 2015. Morphological characteristics observed during early follicular development in perinatal MRL/MpJ mice. *Jpn. J. Vet. Res.* in press.

37. Slot, K. A., M. Voorendt, M. de Boer-Brouwer, H. H. van Vugt, and K. J. Teerds. 2006. Estrous cycle dependent changes in expression and distribution of Fas, Fas ligand, Bcl-2, Bax, and pro- and active caspase-3 in the rat ovary. *J. Endocrinol.* 188: 179–192.

38. Sakamaki, K., H. Yoshida, Y. Nishimura, S. Nishikawa, N. Manabe, and S. Yonehara. 1997. Involvement of fas antigen in ovarian follicular atresia and luteolysis. *Mol. Reprod. Dev.* 47: 11–18.

39. Medeiros, P. B., M. V. Febrônio, E. Bonfá, E. F. Borba, A. D. Takiuti, and C. A. Silva. 2009. Menstrual and hormonal alterations in juvenile systemic lupus erythematosus. *Lupus* 18: 38–43.

40. Shabanova, S. S., L. P. Ananieva, Z. S. Alekberova, and I. I. Guzov. 2008. Ovarian

function and disease activity in patients with systemic lupus erythematosus. *Clin. Exp. Rheumatol.* 26: 436–441.

41. de Araujo, D. B., L. Y. Yamakami, N. E. Aikawa, E. Bonfá, V. S. Viana, S. G. Pasoto, R. M. Pereira, P. C. Serafin, E. F. Borba, and C. A. Silva. 2014. Ovarian reserve in adult patients with childhood-onset lupus: a possible deleterious effect of methotrexate? *Scand. J. Rheumatol*. 43: 503-511.

42. Costenbader, K. H., D. Feskanich, M. J. Stampfer, and E. W. Karlson. 2007. Reproductive and menopausal factors and risk of systemic lupus erythematosus in women. *Arthritis Rheum.* 56: 1251–1262.

Figure Legends

Figure 1. The ratio of spleen weight to body weight in mice.

Each bar represents the mean ± SE (n ≥ 4), and multiple comparisons were performed using a non-parametric Kruskal–Wallis test (Scheffe's method). *: $P < 0.05$, **: $P < 0.01$.

Figure 2. The postnatal date of vaginal opening of mice.

Each bar represents the mean ± SE (n ≥ 4), and multiple comparisons were performed using a non-parametric Kruskal–Wallis test (Scheffe's method). *: $P < 0.05$.

Figure 3. Age-related changes in the estrous cycle in mice.

(**A**) Estrous cycles monitored for 10 consecutive days in C57BL/6, MRL/+, and MRL/lpr mice at 3, 6, 9 and 12 months. Representative cycle traces are shown with days plotted on the X axis. D: diestrus. P: proestrus. E: estrus.

(**B**) The length of estrus, monitored for 10 days, at 3, 6, 9, and 12 months.

(**C**) The length of diestrus, monitored for 10 days, at 3, 6, 9, and 12 months. Each bar represents the mean ± SE (n ≥ 5), and multiple comparisons were performed using a

non-parametric Kruskal–Wallis test (Scheffe's method). *: $P < 0.05$.

Figure 4. Age-related morphological changes in mouse ovaries.

(**A–I**) Whole ovaries of C57BL/6 (A–C), MRL/+ (D–F), and MRL/lpr (G–I) mice at 3 (A, D, and G), 6 (B, E, and H), and 12 (C, F, and I) months. All sections were stained with HE. Asterisks represent corpora lutea (CL). Follicles decreased in number with age in all strains (A–I); the decrease was most severe in MRL/lpr mice (G–I). Fewer corpora lutea and an ovarian interstitium with a larger area were observed in MRL/lpr mice (G–I) compared to the other strains. Bars = 200 μm.

(**J–M**) The number of follicles at each stage at 3 (J), 6 (K), and 12 (L) months, and the number of CL at each age (M). The number of follicles and corpora lutea was counted in five sections. The total number in all five sections was used as the value for that ovary. Each bar represents the mean ± SE (n = 4), and multiple comparisons were performed using a non-parametric Kruskal–Wallis test (Scheffe's method). *: $P < 0.05$.

Figure 5. Age-related histological changes in the ovarian interstitium and surface epithelium in mice.

(**A–I**) Ovarian cortices of C57BL/6 (A-C), MRL/+ (D–F), and MRL/lpr (G–I) mice at 3

584 (A, D, and G), 6 (B, E, and H), and 12 (C, F, and I) months. All sections were stained
585 with PAS stain. Asterisks indicate interstitial glands composed of interstitial endocrine
586 cells. Fully developed interstitial glands were observed in C57BL/6 mice ovaries at 12
587 months (C), in MRL/+ mice at 6 (E) and 12 (F) months, and in MRL/lpr mice at 3 (G), 6
588 (H), and 12 (I) months.
589 (**J–L**) Ovarian cortices of C57BL/6 (J), MRL/+ (K), and MRL/lpr (L) mice at 6 months.
590 All sections were stained with HE. A squamous, monolayered epithelium covered the
591 ovarian surface in C57BL/6 (J) and MRL/+ (K) mice. Cuboidal and stratified surface
592 epithelial cells (arrowheads) were observed in MRL/lpr mice (L). Bars = 100 μm.
593
594 **Figure 6. Ultrastructure of mouse ovaries.**
595 (**A–D**) Ultrastructure of the ovarian surface under SEM observation in C57BL/6 (A and
596 B) and MRL/lpr (C and D) mice at 6 months. The ovarian surface of C57BL/6 mice was
597 smooth (A) and covered with oval epithelial cells (arrowheads) or spindle-shaped cells
598 (arrows) with microvilli (B). The ovarian surface of MRL/lpr mice showed several
599 dome-shaped bulges (C), and was mostly covered with round epithelial cells with
600 abundant microvilli (D). The insets show ovarian epithelial cells at a higher
601 magnification. Black bars = 200 μm. White bars = 20 μm. Inset bars = 5 μm.

(**E–H**) Ultrastructure of the ovarian surface in C57BL/6 (E and F) and MRL/lpr (G and H) mice at 6 months. Semi-thin sections under light microscopy (E and G) and ultra-thin sections under TEM (F and H) are shown. The yellow dotted lines indicate the basal membrane (E–H). Two cell types, pale-colored cells (black arrows) and black-colored cells (arrowheads), were observed in the superficial epithelium of C57BL/6 (E) and MRL/lpr (G) mice. The tunica albuginea (dual-headed yellow arrows) were thicker in MRL/lpr mice than in C57BL/6 mice (E and G). In the ovarian surface epithelium of C57BL/6 mice (F), the round cells contained large nuclei, a few microvilli, and a cytoplasm with a low electron density (arrowhead), whereas squamous cells had abundant microvilli and an electron-dense cytoplasm (arrows). In the ovarian surface epithelium of MRL/lpr mice (H), all cells were taller than those of C57BL/6 mice (F and H), and cells with few microvilli and a cytoplasm with a low electron density bulged toward the peritoneal cavity (arrowheads). Thickened tunica albuginea in MRL/lpr mice contained numerous collagen fibers (H, asterisks). Similar to C57BL/6 mice, cells with abundant microvilli and an electron-dense cytoplasm (arrows) were observed, and its density appeared to be higher than in C57BL/6 mice (F and H). Bars = 10 μm.

Figure 7. Characteristics of cell infiltration in mouse ovaries.

(**A–C**) The localization of CD3-positive T cells in the ovaries of C57BL/6 (A), MRL/+ (B), and MRL/lpr (C) mice at 6 months. A few positive cells were observed in or around the corpora lutea of C57BL/6 (A) and MRL/+ (B) mice. Numerous positive cells were observed in the ovaries of MRL/lpr mice; these were widely distributed but were mainly localized to the ovarian interstitium (C).

(**D**) The number of CD3-positive T cells at 3 and 6 months in the ovaries of C57BL/6, MRL/+, and MRL/lpr mice. The number of positive cells was counted in five sections. The total number in all five sections was used as the value for that ovary. Each bar represents the mean ± SE ($n \geq 3$), and multiple comparisons were performed using a non-parametric Kruskal–Wallis test (Scheffe's method). *: $P < 0.05$, **: $P < 0.01$.

(**E–F**) The characteristic localization of CD3-positive cells in the ovaries of MRL/lpr mice at 3 months of age. Positive cells were mainly localized in or around atretic (E, arrowhead) and primordial follicles (F).

(**G–I**) The localization of B220-positive cells in the ovaries of C57BL/6 (G), MRL/+ (H), and MRL/lpr (I) mice at 6 months. Numerous positive cells were observed in the ovarian interstitium of MRL/lpr mice (I). Bars = 50 μm.

Figure 8. The serum concentrations of FSH and testosterone in female mice.

(**A**) The serum concentration of FSH in female C57BL/6, MRL/+, and MRL/lpr mice at 6 and 12 months.

(**B**) The serum concentration of testosterone in female C57BL/6, MRL/+, and MRL/lpr mice at 6 and 12 months. Each bar represents the mean ± SE ($n \geq 4$).

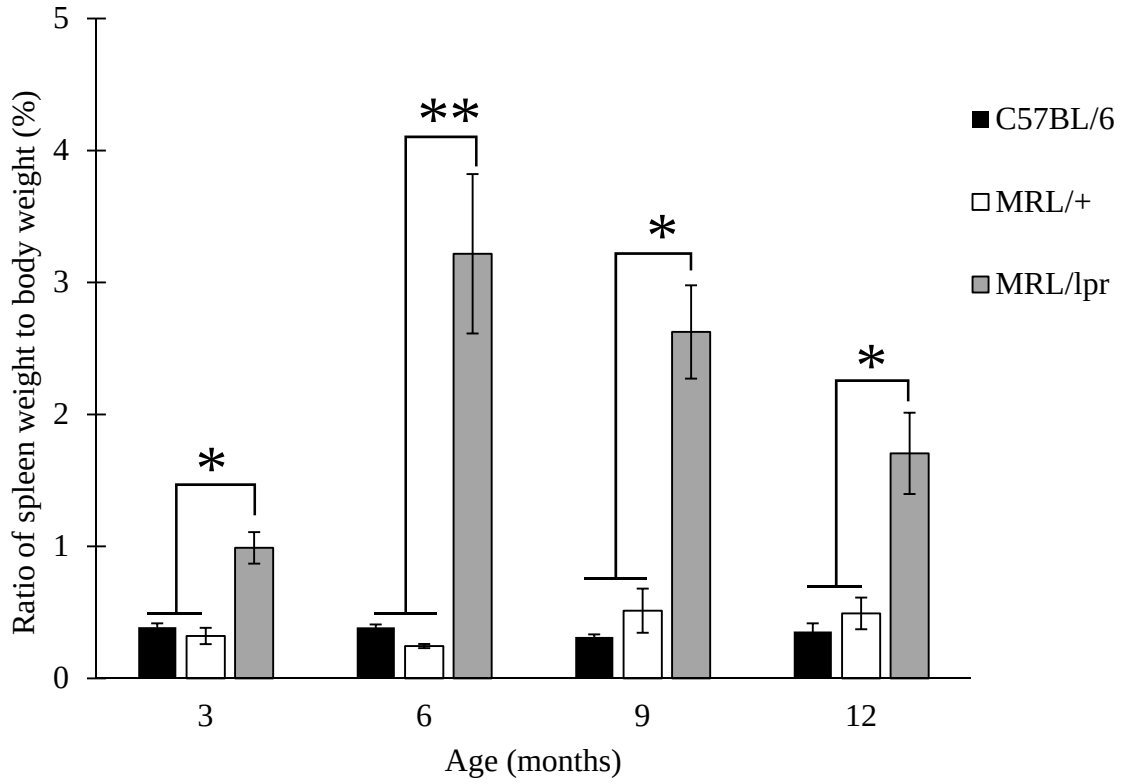
Ratio of spleen weight to body weight (%)
5
4
3
2
1
0
**
*
*
*
C57BL/6
MRL/+
MRL/lpr
3
6
9
12
Age (months)

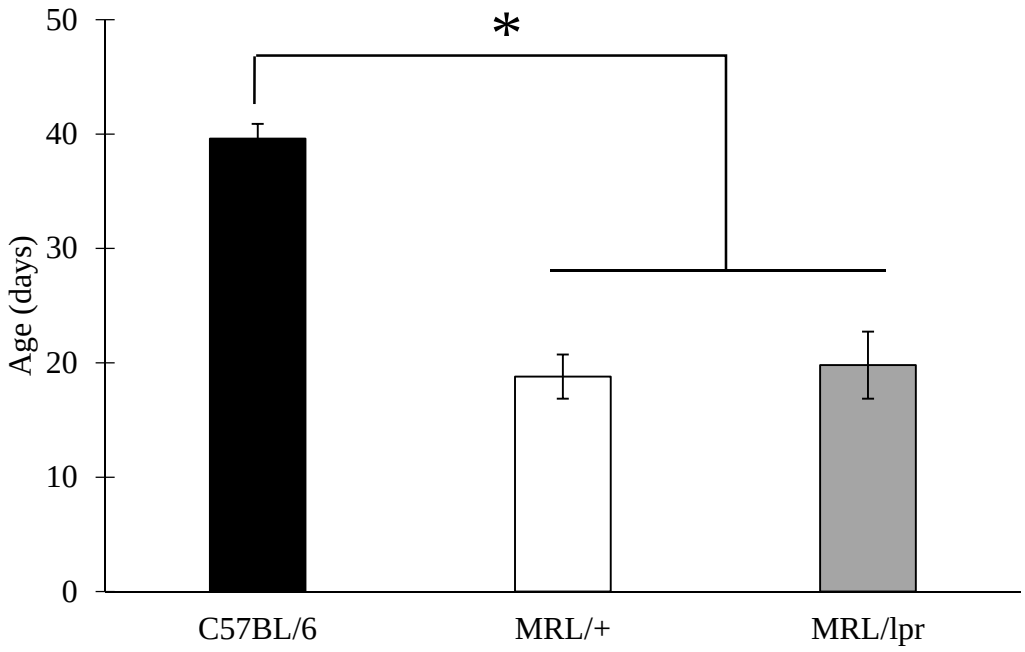
50
40
30
20
10
0
Age (days)
*
C57BL/6
MRL/+
MRL/lpr

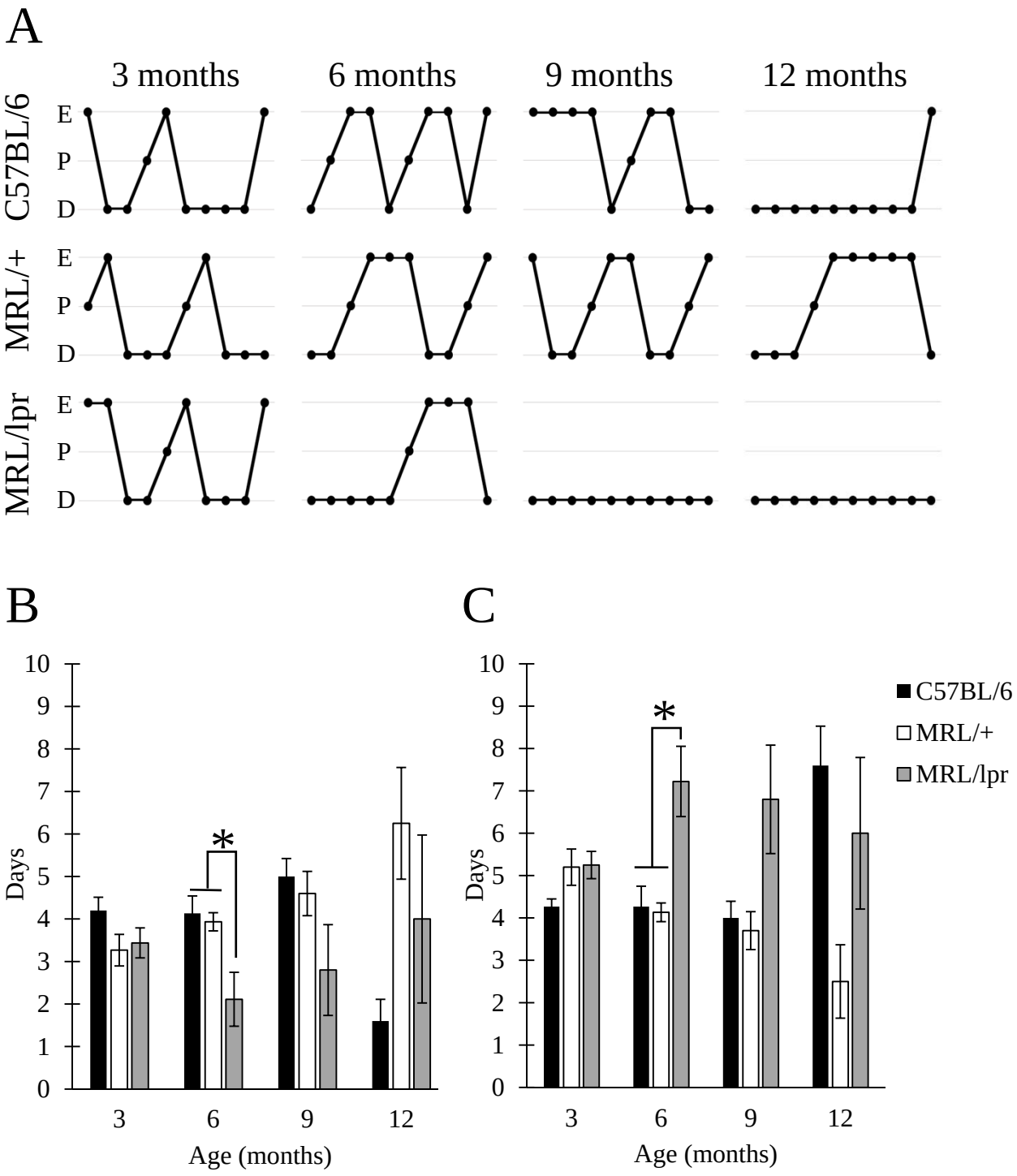
A
3 months
6 months
9 months
12 months
C57BL/6
MRL/+
MRL/lpr
E
P
D
B
C
Days
Age (months)
3
6
9
12
*
C57BL/6
MRL/+
MRL/lpr

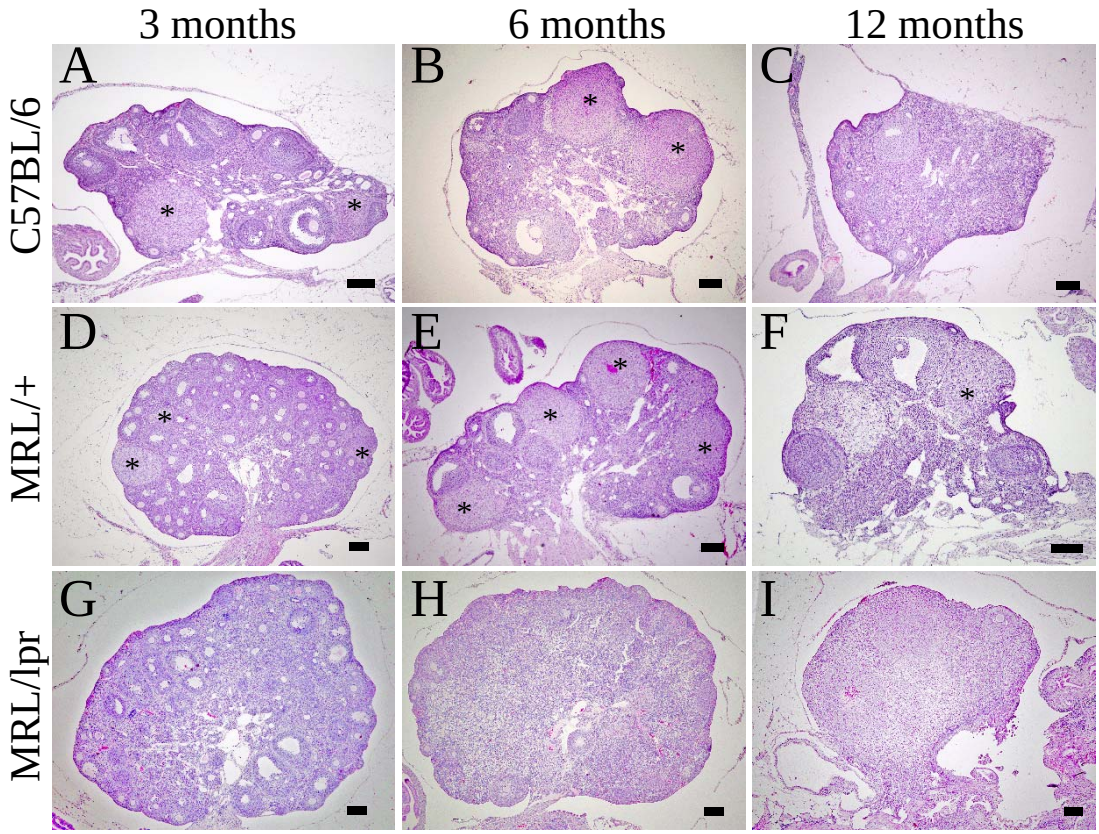
3 months
6 months
12 months
C57BL/6
MRL/+
MRL/lpr
A
B
C
D
E
F
G
H
I

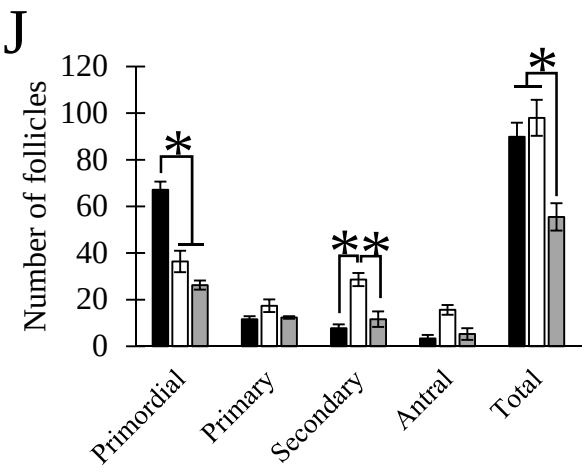
J
Number of follicles
120
100
80
60
40
20
0
Primordial
Primary
Secondary
Antral
Total

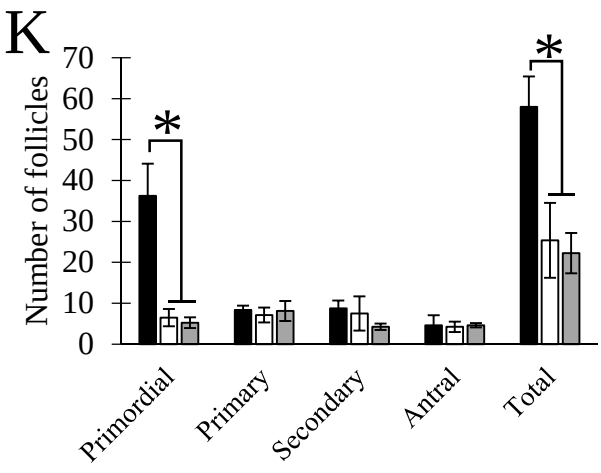
K
Number of follicles
70
60
50
40
30
20
10
0
Primordial
Primary
Secondary
Antral
Total

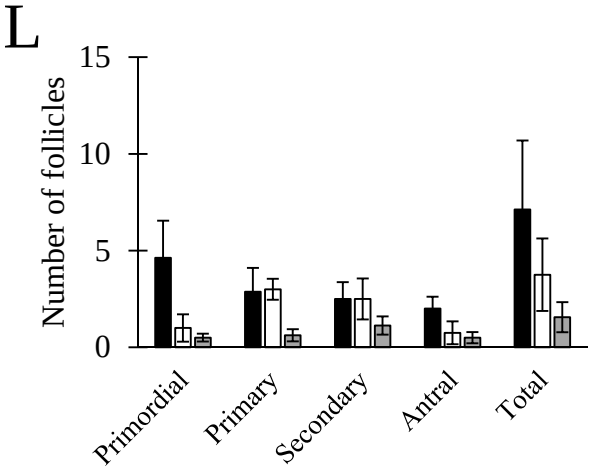
L
Number of follicles
15
10
5
0
Primordial
Primary
Secondary
Antral
Total

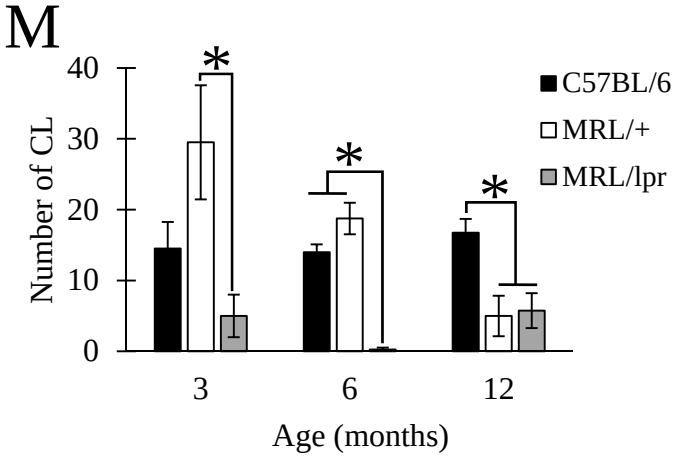
M
Number of CL
40
30
20
10
0
3
6
12
Age (months)
C57BL/6
MRL/+
MRL/lpr

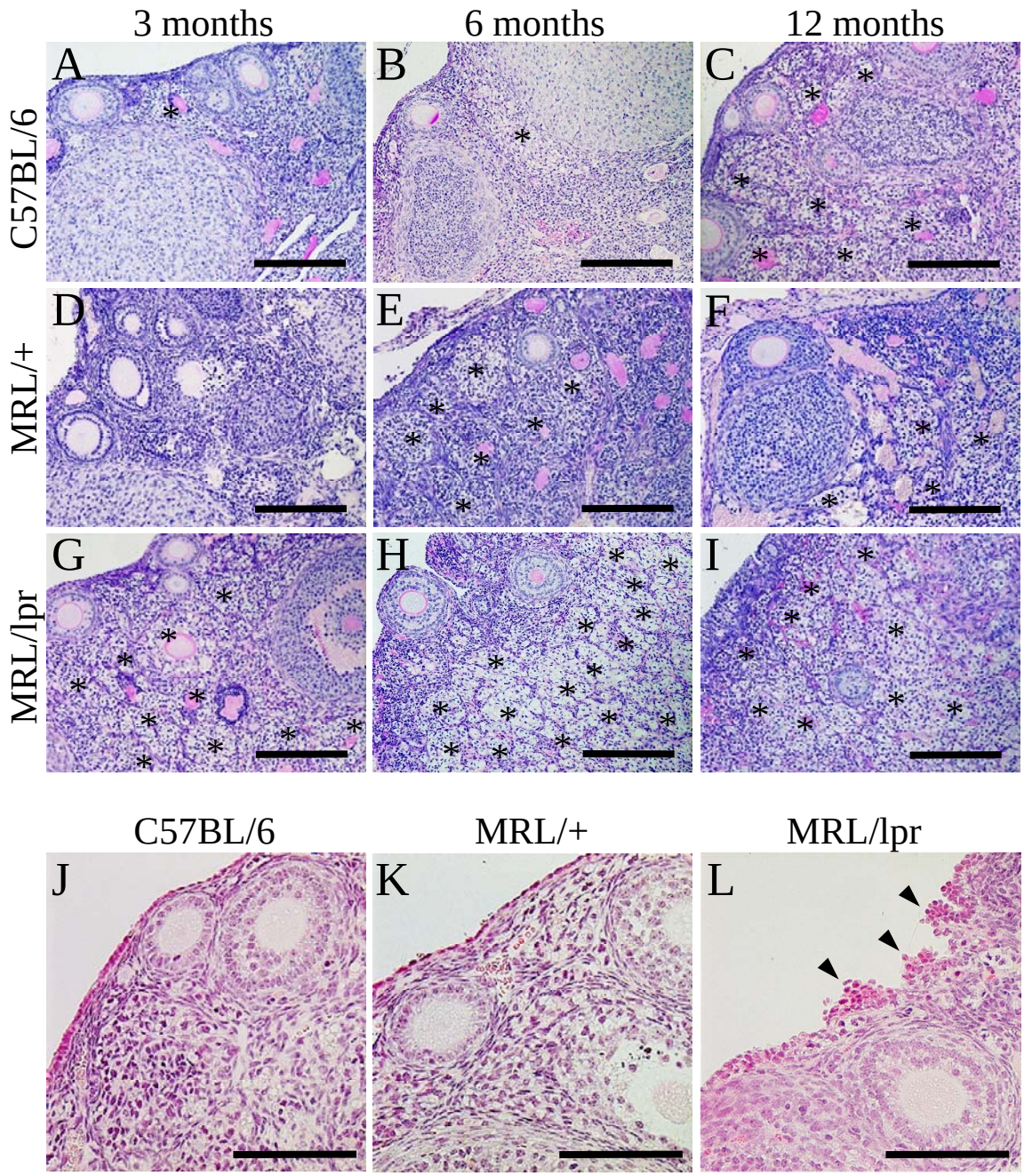
3 months
6 months
12 months
C57BL/6
MRL/+
MRL/lpr
A
B
C
D
E
F
G
H
I
C57BL/6
MRL/+
MRL/lpr
J
K
L

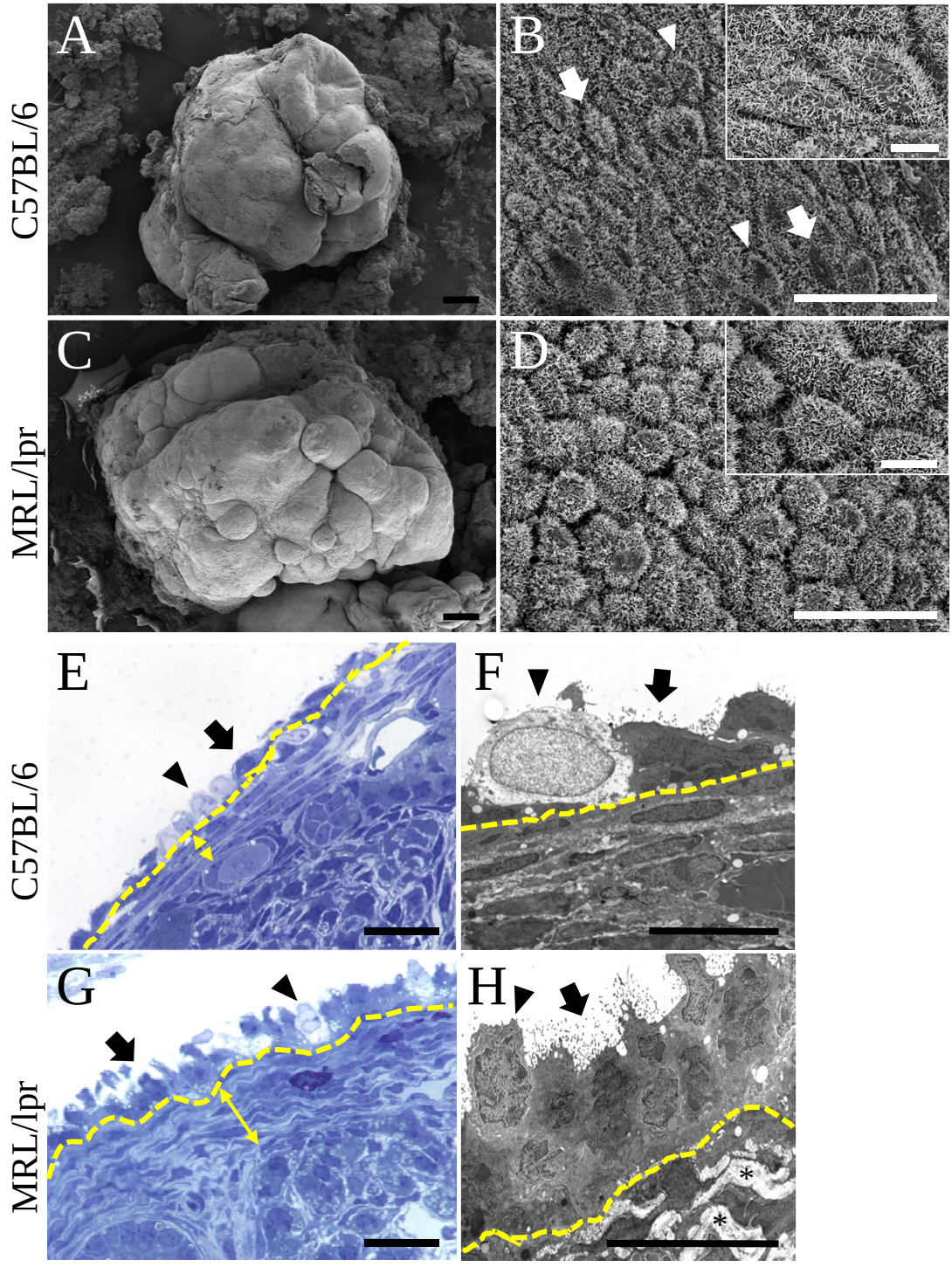
C57BL/6
MRL/lpr
A
B
C
D
C57BL/6
MRL/lpr
E
F
G
H
*
*

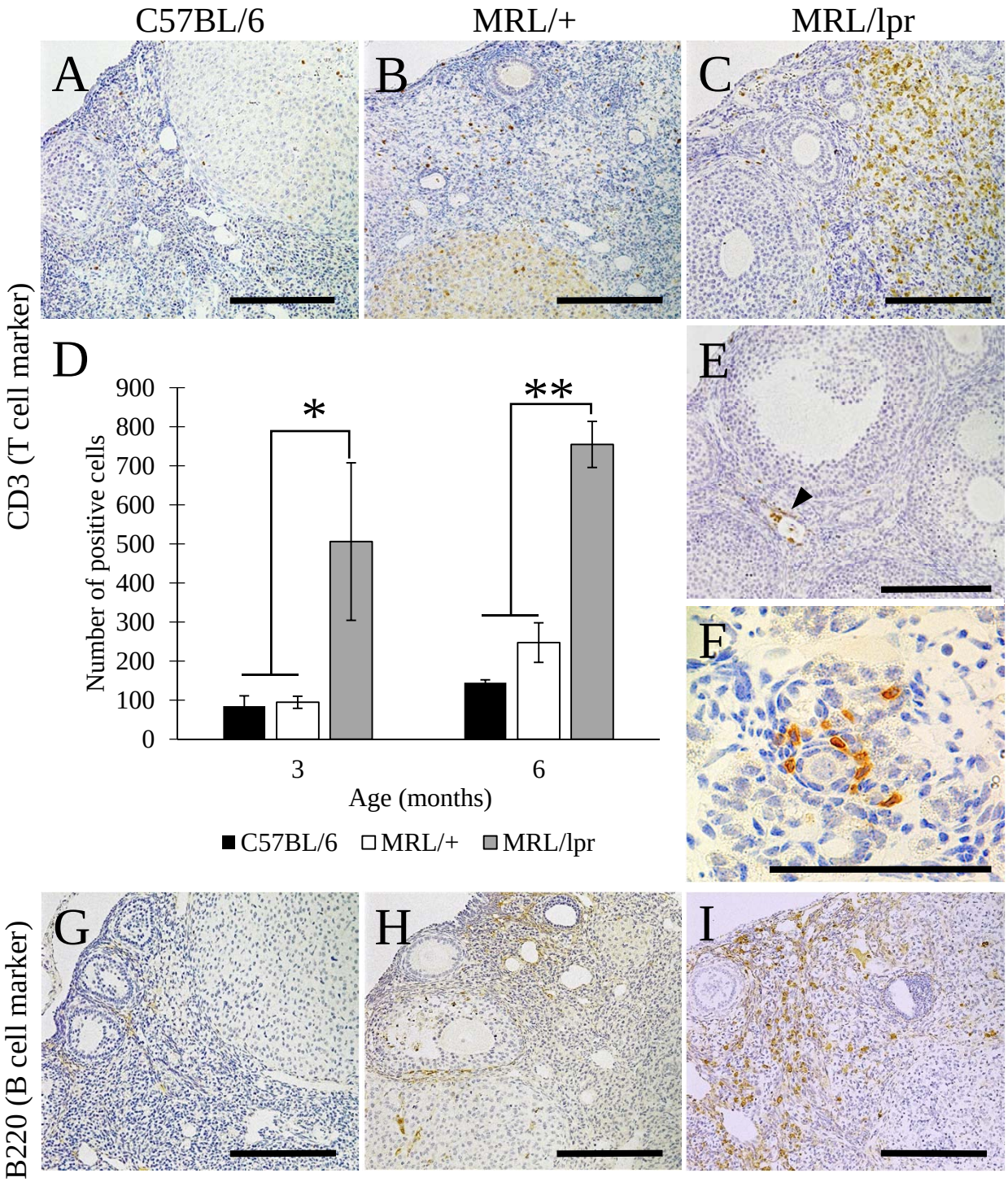
C57BL/6
MRL/+
MRL/lpr
A
B
C
CD3 (T cell marker)
D
E
F
900
800
700
600
500
400
300
200
100
0
Number of positive cells
*
**
3
6
Age (months)
C57BL/6
MRL/+
MRL/lpr
B220 (B cell marker)
G
H
I

A

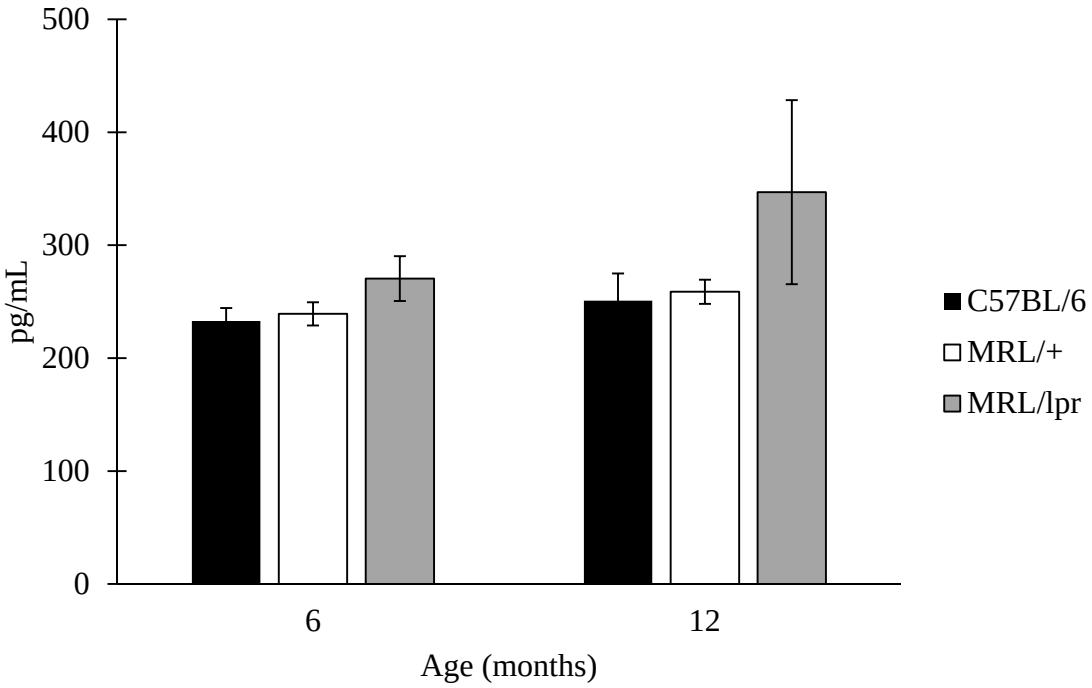
500
400
300
200
100
0
pg/mL
6
12
Age (months)
C57BL/6
MRL/+
MRL/lpr

B

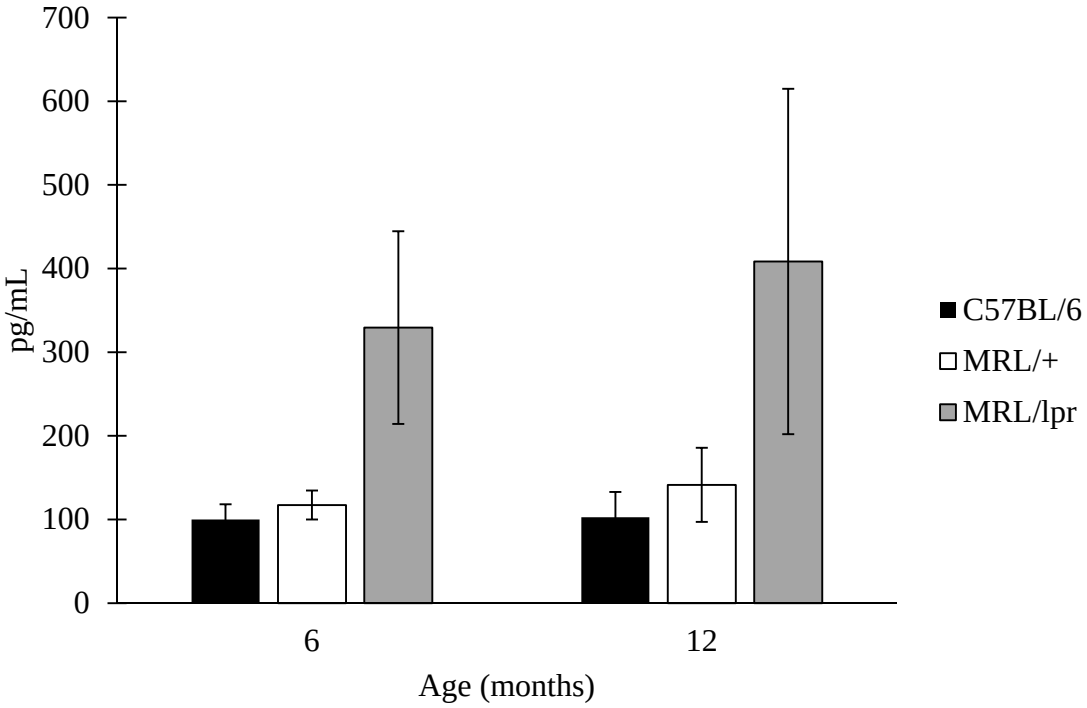
700
600
500
400
300
200
100
0
pg/mL
6
12
Age (months)
C57BL/6
MRL/+
MRL/lpr